

1 **Synchronous emplacement of the anorthosite
2 xenolith-bearing Beaver River diabase and one of the
3 largest lava flows on Earth**

4 **Yiming Zhang¹, Nicholas L. Swanson-Hysell¹, Mark D. Schmitz², James D.
5 Miller Jr.³, Margaret S. Avery^{1,4}**

6 ¹Department of Earth and Planetary Science, University of California, Berkeley, CA, USA

7 ²Department of Geosciences, Boise State University, Boise, ID, USA

8 ³Department of Earth and Environmental Sciences, University of Minnesota, Duluth, MN, USA

9 ⁴Geology, Minerals, Energy, and Geophysics Science Center, U.S. Geological Survey, Moffett Field, CA,
10 USA

11 **Key Points:**

- 12 • New geochronology precisely constrain the timing of emplacement of anorthosite
13 xenoliths within the Beaver River diabase of the Midcontinent Rift.
- 14 • Paleomagnetic and geochronological data support that the Beaver River diabase
15 is comagmatic with the very high volume Greenstone Flow.
- 16 • Wide conduits of magma to the surface are indicated by large anorthosite xeno-
17 liths.

18 **Abstract**

19 New geochronologic and paleomagnetic data from the North American Midcontinent Rift
 20 (MCR) reveal the synchronous emplacement of the Beaver River diabase, the anorthosite
 21 xenoliths within it, and the Greenstone Flow — one of the largest lava flows on Earth.
 22 A U-Pb zircon date of 1091.83 ± 0.21 Ma from one of the anorthosite xenoliths is con-
 23 sistent with the anorthosite cumulate forming as part of the Midcontinent Rift and pro-
 24 vides a maximum age constraint for the Beaver River diabase. Paired with the minimum
 25 age constraint of a cross-cutting Silver Bay intrusion (1091.61 ± 0.14 Ma) these data tightly
 26 bracket the age of the Beaver River diabase to be 1091.7 ± 0.2 Ma (95% CI), coeval with
 27 the eruption of the Greenstone Flow — which is further supported by indistinguishable
 28 tilt-corrected paleomagnetic pole positions. These data, as well as mineralogical and geo-
 29 chemical data, support the hypothesis that the Beaver River diabase that entrained large
 30 anorthosite xenoliths was the feeder system for the Greenstone Flow. The large areal ex-
 31 tent of the intrusives and large estimated volume of the volcanics suggest that they rep-
 32 resent a rapid and voluminous *ca.* 1092 Ma magmatic pulse near the end of the main
 33 stage of MCR magmatism.

34 **1 Introduction**

35 The North American Midcontinent Rift (MCR) is a *ca.* 1.1 Ga large igneous province
 36 for which there is excellent exposure of both the intrusive and extrusive components in
 37 the Lake Superior region (Fig. 1). An exceptional feature of the Midcontinent Rift is the
 38 occurrence of large anorthosite xenoliths (whose diameter can exceed 150 meters) within
 39 a diabase sill and dike network known as the Beaver River diabase that outcrops in north-
 40 eastern Minnesota, USA, as part of the Beaver Bay Complex (Fig. 1). Despite these anorthosite
 41 xenoliths having long been recognized and mapped, the origin of these nearly pure pla-
 42 gioclase cumulates has been debated in the literature (Lawson, 1893; Grout, 1939; Mor-
 43 rison et al., 1983; Miller & Chandler, 1997). Lacking the roadcut exposures that now make
 44 the xenolithic relationship clear and observing the large blocks exposed along the Lake
 45 Superior shoreline and at Carlton Peak, Lawson (1893) did not recognize the anorthosites
 46 as xenoliths. Rather, he argued that the anorthosite is Archean in age and that the Ke-
 47 weenawan (i.e. Midcontinent Rift related) magma was emplaced atop an anorthosite ero-
 48 sional unconformity surface. Later work established the anorthosite blocks as xenoliths,
 49 which are now extensively documented through geologic mapping of the region (Fig. 1;

50 Miller et al. (2001); Miller (1988); Miller and Boerboom (1989); Boerboom (2004); Boer-
51 boom and Green (2006); Boerboom et al. (2006, 2007)) and outcrop-scale exposures (Fig.
52 3).

53 The anorthosite xenoliths range in size from centimeter-scale megacrysts to meter-
54 scale, decimeter-scale and even >150 meter-scale blocks (Fig. 3; Morrison et al. (1983);
55 Grout (1939)). There have been divergent interpretations regarding the age and magma
56 source of these anorthosite xenoliths (Fig. 1). Grout (1939) recognized the xenolithic na-
57 ture of the anorthosites and suggested that the massive intrusion of the older anorthositic
58 gabbro within the Duluth Complex may have supplied anorthosite fragments that were
59 later entrained by the Beaver River diabase emplacement. However, the distinctive modes,
60 textures, mineral chemistry, and trace element and isotopic (Sm-Nd, Rb-Sr) composi-
61 tions between the anorthosite xenoliths and the *ca.* 1096 Ma Anorthositic Series of the
62 Duluth Complex challenge this interpretation. Morrison et al. (1983), on the other hand,
63 argued that the xenoliths were sourced from Paleoproterozoic or Archean lower crust that
64 were liberated and contaminated by Midcontinent Rift magmas based on Sm and Nd iso-
65 topic data. They interpreted a Sm-Nd model age of 1.9 Ga from one of the xenoliths as
66 providing a minimum crystallization age for the anorthosites though they acknowledged
67 that these constraints are not definitive with respect to the age.

68 In contrast to this Archean to Paleoproterozoic model, Miller and Chandler (1997)
69 favored a scenario where the anorthosite crystallized as part of Midcontinent Rift mag-
70 matism. They cited work by Kushiro (1980) who showed that the changing density con-
71 trast between labradoritic to bytownitic plagioclase and tholeiitic magma at different crustal
72 pressures would promote flotation of plagioclase in deep (>20 km) crustal magma cham-
73 bers and the creation of anorthosite cumulates in the lower crust. This mechanism of
74 plagioclase flotation likely created massive anorthosite cumulates in the roof zones of sub-
75 crustal magma chambers during MCR magmatism. Miller and Weiblen (1990) specu-
76 lated that plagioclase-phyric magmas tapped from these deep chambers fed shallow (~5km)
77 subvolcanic intrusions of the Duluth Complex, thereby creating the anorthositic gabbros
78 of the Anorthositic Series. Miller and Chandler (1997) suggested that the nearly pure
79 anorthosite xenoliths occurring in the younger and more hypabyssal diabase intrusions
80 of the Beaver Bay Complex were harvested from these phase-segregated intrusions in the
81 lower crust. They further argued that the isotopic data of Morrison et al. (1983) can be
82 explained by anorthosite-forming MCR magmas having been contaminated by older crust

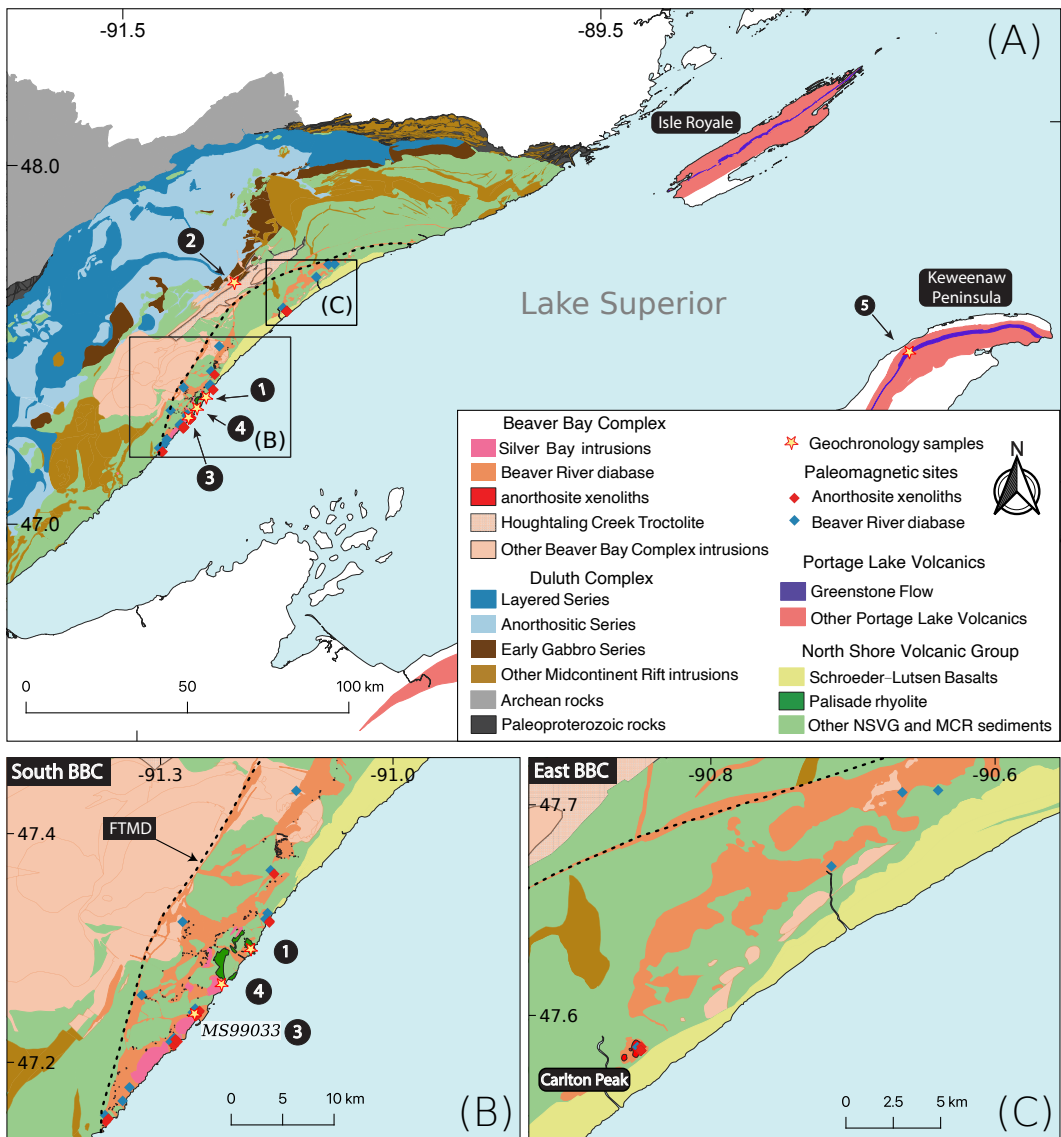


Figure 1: (A) Geologic map of exposures of Midcontinent Rift volcanics and intrusives in the western Lake Superior region. The Greenstone Flow (purple) of the Portage Lake Volcanics (red) outcrops throughout the Keweenaw Peninsula and Isle Royale. (B) Regional map of paleomagnetic and geochronologic sites in the southern Beaver Bay Complex (south BBC). Note that paleomagnetic site AX16 and geochronology sample MS99033 are from the same anorthosite xenolith. The geochronology sample numbers in (A) and (B) correspond to those in Fig. 4. (C) Regional map of paleomagnetic sites in the eastern Beaver Bay Complex (east BBC). The xenolith at Carlton Peak is >100 meters in diameter. The younger Schroeder-Lutsen basalt of the North Shore Volcanic Group (NSVG) is lying unconformably atop the Beaver River diabase and other NSVG units. The nomenclature of the “southern” and “eastern” Beaver Bay Complex follows Miller and Chandler (1997). FTMD - Finland tectonomagmatic discontinuity, traced out by the dashed black line. Bedrock geology is from Miller et al. (2001) and Jirsa et al. (2011).

83 rather than the anorthosites being older lower crust that was contaminated by MCR mag-
84 mas.

85 Regardless of their origin, the exceptional sizes of some of the anorthosite xeno-
86 liths reveal the immense widths of the Beaver River diabase conduits. A particularly large
87 anorthosite xenolith is exposed at Carlton Peak in the eastern Beaver Bay Complex with
88 minimum dimensions of 180×240 meters (Fig. 1, 3; Boerboom et al. (2006)). In the
89 southern Beaver Bay Complex, a large anorthosite xenolith near Corundum Point has
90 dimensions of 180×230 meters while the one exposed at Split Rock Point has dimen-
91 sions of 180×260 meters (Boerboom, 2004). To be able to accommodate such large xeno-
92 liths during magma ascent from the lower crust, the Beaver River diabase conduits must
93 have been of at least the width of the anorthosite short axis diameters. Such wide con-
94 ducts in these near-surface intrusions suggest high magma flux rates and make it likely
95 that the magma extruded to the surface — feeding voluminous lava flows.

96 Miller and Chandler (1997) emphasized the composite nature of the Beaver River
97 diabase network and Silver Bay intrusions (Fig. 1), which are locally marked by abrupt
98 transitions to progressively more evolved lithologies. Furthermore, that study documented
99 geochronologic, geochemical and structural evidence to support the notion that the di-
100 abase network may have served as principal feeder conduits to lava flows including parts
101 of the Portage Lake Volcanics on the Keweenaw Peninsula and Isle Royale of Michigan
102 (Fig. 1). To more directly test this inferred intrusive-extrusive correlation, Doyle (2016)
103 compared the mineralogical, textural, and geochemical attributes and the composite litho-
104 logic nature of the Beaver River diabase against those of the Greenstone Flow, the largest
105 lava flow within the Midcontinent Rift and one of the largest lava flows on Earth (Fig.
106 2). The Greenstone Flow also has a composite nature, which is indicated by its litho-
107 logic zonation of ophitic basalt forming the upper and lower zones and an interior zone
108 composed of prismatic ferrogabbro to granophyric monzodiorite. Doyle (2016) documented
109 remarkable similarities in petrography, mineral chemistry, whole rock geochemistry, and
110 lithologic zonation between the Beaver River diabase intrusions in northern Minnesota
111 and the Greenstone Flow on both Isle Royale and Keweenaw Peninsula. Based on the
112 interpreted feeder system being in northern Minnesota, Doyle (2016) estimated the full
113 extent of the Greenstone Flow to be ~ 20000 km 2 and its volume to be between 2000 and
114 6000 km 3 (Fig. 2).

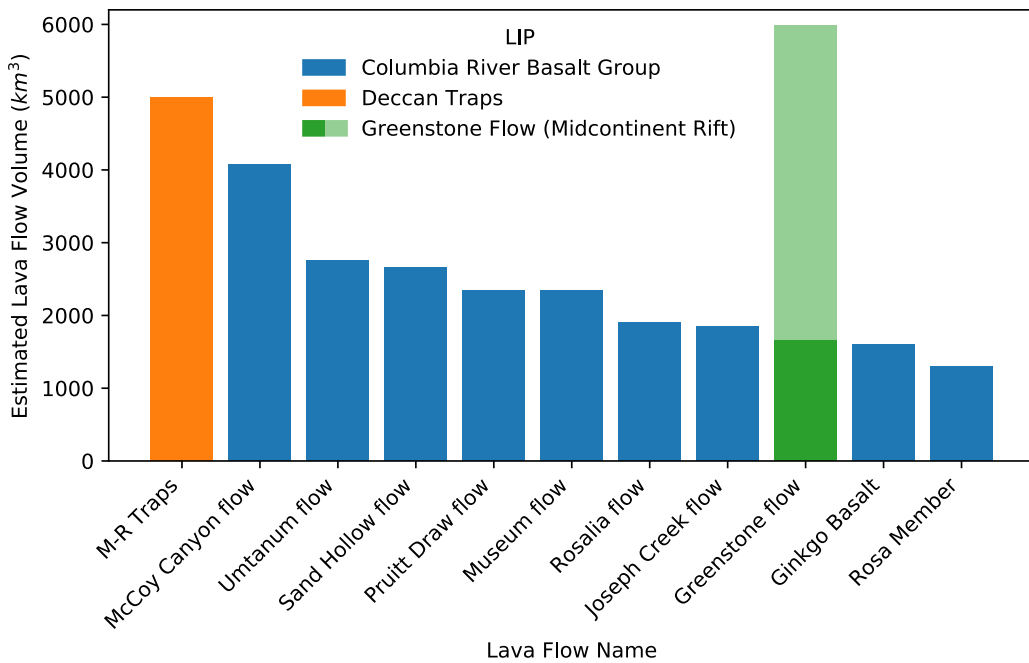


Figure 2: Bar plot of ten of the world's most voluminous single mafic lava flows currently known. With an estimated minimum volume of $\sim 1650 \text{ km}^3$ and likely volume as high as $\sim 6000 \text{ km}^3$, the Greenstone Flow from the 1.1 Ga Midcontinent Rift stands amongst the giant lava flows from the Deccan Traps and Columbia River basalts. M-R Traps = Mahabaleshwar–Rajahmundry lava flow in the Deccan Traps. Data from Self et al. (2008), Bryan et al. (2010), Longo (1984), and Doyle (2016).

A comagmatic relationship between the Beaver River diabase and the Greenstone Flow is consistent with the similar $^{207}\text{Pb}/^{206}\text{Pb}$ dates developed from a granophyric ferrogabbro within the Beaver Bay Complex (1095.8 ± 1.2 Ma, Paces and Miller (1993)) and the Greenstone Flow (1094.0 ± 1.5 Ma, Davis and Paces (1990)). The relatively large uncertainties provided by the existing $^{207}\text{Pb}/^{206}\text{Pb}$ geochronology more roughly constrains the temporal relationships between these rapid events than is possible with modern methods. Modern-day U-Pb geochronology techniques for isotope dilution-thermal ionization mass spectrometry (ID-TIMS) allow high precision $^{206}\text{Pb}/^{238}\text{U}$ dates to be developed from chemically-abraded zircon crystals (Mattinson, 2005). Studies utilizing these methods on Midcontinent Rift volcanics and intrusions have shown that the analytical uncertainties on weighted mean $^{206}\text{Pb}/^{238}\text{U}$ dates of multiple chemically-abraded single zircons can be of ~ 200 kyr, an order of magnitude smaller than previous dates that are based exclusively on the $^{207}\text{Pb}/^{206}\text{Pb}$ system (Fairchild et al., 2017; Swanson-Hysell et al., 2019, 2020). These $^{206}\text{Pb}/^{238}\text{U}$ dates are also considered to be more accurate than systematically older $^{207}\text{Pb}/^{206}\text{Pb}$ dates (Schoene et al., 2006). Such $^{238}\text{U}/^{206}\text{Pb}$ dates have revealed that the massive Layered Series and Anorthositic Series rocks of the Duluth Complex were emplaced in ~ 500 kyr *ca.* 1096 Ma (Swanson-Hysell et al., 2020).

In this work, we use a new $^{206}\text{Pb}/^{238}\text{U}$ zircon date for an anorthosite xenolith within the Beaver River diabase, in conjunction with $^{206}\text{Pb}/^{238}\text{U}$ dates from a Silver Bay intrusion and the Greenstone Flow (Fig. 1; Fairchild et al. (2017)), to evaluate the timing of emplacement of the Beaver River diabase, and the hypothesized intrusive-extrusive correlation between the Beaver River diabase and the Greenstone Flow.

Paleomagnetic data can also provide chronological constraints on rock units. Laurentia experienced a period of rapid latitudinal plate motion during rift development (Swanson-Hysell et al., 2009). A synthesized apparent polar wander path (APWP) based on the Midcontinent Rift volcanic rocks indicates that motion exceeded 20 cm/yr (Swanson-Hysell et al., 2019), faster than the maximum speed of India of ~ 17 cm/yr during the Cenozoic (van Hinsbergen et al., 2011). This motion resulted in significant differences in pole positions recorded by Midcontinent Rift rocks that were emplaced a few million years apart (Swanson-Hysell et al., 2019). In this study, we present paleomagnetic data from the anorthosite xenoliths and the host Beaver River diabase. Data from the xenoliths give equivalent directions to the host diabase (Figs. 5, 6), indicating that they were heated above the Curie temperature of magnetite and acquired a thermal remanent mag-

netization when they cooled with the diabase. This thermal history is consistent with thermal diffusion modeling of the xenoliths. The paleomagnetic data can be compared to data from the Greenstone Flow to further test the hypothesis that they are synchronous. The resulting paleomagnetic pole positions can also be compared to the synthesized Laurentia APWP to obtain chronological constraints (Fig. 6).

Here, by integrating the geochronologic and paleomagnetic perspectives with previous lithologic and geochemical analyses (Miller & Chandler, 1997; Doyle, 2016), we more definitely establish that the Beaver River diabase network acted as the feeder system for the Greenstone Flow of the Portage lake Volcanic-equivalent flows. Their shared geochemical signatures, composite nature of emplacement, and the inference of giant magma conduits that transported large anorthositic xenoliths characterize a period of *ca.* 1092 Ma voluminous magmatic activity (based on $^{206}\text{Pb}/^{238}\text{U}$ zircon dates; Fig. 1).

2 Geologic Setting

2.1 Beaver Bay Complex and Related Rocks of NE Minnesota

The North American Midcontinent Rift (MCR) is a failed intracontinental rift where protracted magmatic activity lasted from *ca.* 1109 Ma to *ca.* 1084 Ma (Swanson-Hysell et al., 2019). Midcontinent Rift rocks extensively outcrop in today's Lake Superior region, with the total extent traceable by arcuate magnetic and gravity anomalies that extend to the southwest to Kansas, and to the southeast, to southern Michigan (Hinze & Chandler, 2020). Previous studies have divided magmatic activity in the rift into four stages based on interpreted changes in relative magmatic volume and the nature of magmatism: early (\sim 1109–1104 Ma), latent (\sim 1104–1098 Ma), main (\sim 1098–1090 Ma) and late (\sim 1090–1083 Ma) (Vervoort et al., 2007; Heaman et al., 2007; Miller & Nicholson, 2013). In northeastern Minnesota, the Early Gabbro Series and the Felsic Series rocks of the Duluth Complex and reversed-polarity lavas of the lower North Shore Volcanic Group were emplaced during the early stage. The more voluminous Duluth Complex Layered Series and the plagioclase-rich Anorthositic Series, together with an associated \sim 8 km thick extrusive volcanic sequences of the North Shore Volcanic Group (NSVG), were rapidly emplaced about 10 myr later at *ca.* 1096 Ma during the main stage (Paces & Miller, 1993; Swanson-Hysell et al., 2020).

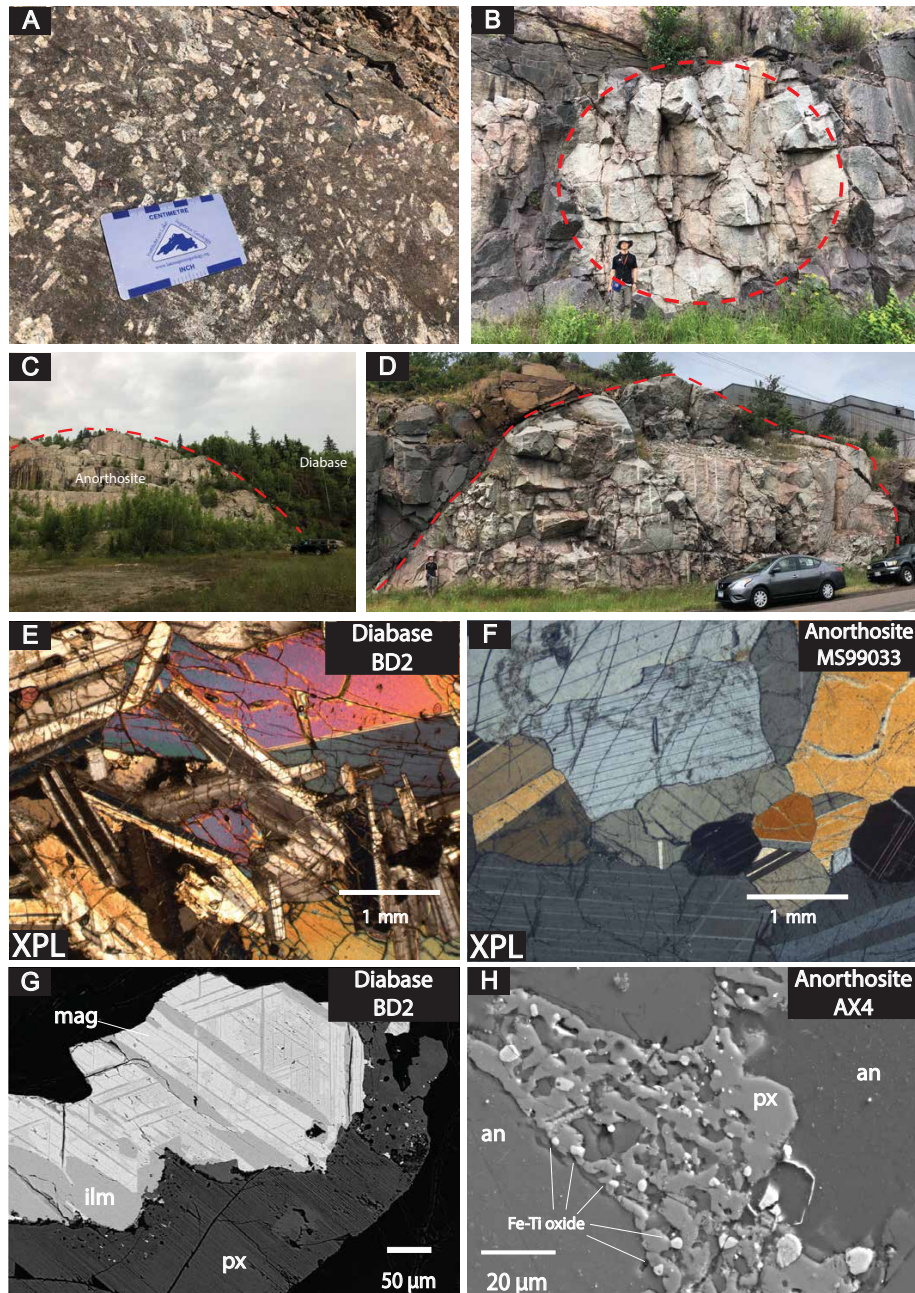


Figure 3: Field photographs and petrographic images of the Beaver River diabase and the anorthosite xenoliths within it. (A) Centimeter-sized plagioclase megacrysts in the diabase. (B) Rounded anorthosite xenolith with a diameter of ~ 7 meters fully entombed within the diabase. (C) Exposure of a giant Carlton Peak anorthosite with a diameter >100 m. (D) 27.5 m diameter anorthosite xenolith sampled as paleomagnetic site AX16 and geochronology sample MS99033. (E) Cross polarized (XPL) image of the subophitic texture of diabase at site BD2 (pyroxene partially enclosing plagioclase). (F) XPL image of anorthosite geochronology sample MS99033. Plagioclase crystals exhibit both granoblastic texture and interlocking lath with fabrics. (G) Back scattered electron (BSE) image of a large Fe-Ti oxide with titanomagnetite-ilmenite lamellae in diabase BD2. (H) BSE image of micron-sized Fe-Ti oxides exsolved from pyroxene between plagioclase crystals in anorthosite AX4.

The Beaver Bay Complex, which sits stratigraphically above the Duluth Complex, is another intrusive complex that resulted from main stage magmatism. The exposed area of the Beaver Bay Complex is $\sim 1000 \text{ km}^2$ where it has been mapped along the north-western shore of Lake Superior in northeastern Minnesota (Fig. 1; Supporting Information). The Beaver Bay Complex is a multi-phase, composite intrusive complex that intrudes parts of the NSVG (Fig. 1; Miller and Chandler (1997); Swanson-Hysell et al. (2020)). Distinct from the deep plutonic intrusions of the Duluth Complex, the majority of the Beaver Bay Complex is formed of hypabyssal intrusions that were emplaced as dikes and sills at shallow depths (Miller & Chandler, 1997). Detailed mapping and petrological analyses of the Beaver Bay Complex has led to the identification of thirteen intrusive units and at least six major intrusive events (Miller & Chandler, 1997). Most of the Beaver Bay Complex intrusions are dioritic to gabbroic in composition, with a trend of becoming progressively less evolved in younger intrusions (Miller & Chandler, 1997). The main lithology of the Beaver River diabase dikes and sills network within the Beaver Bay Complex is an ophitic olivine gabbro (Fig. 3), but in wider areas of dikes and the upper parts of thick sills, this rock type can abruptly transition into intergranular olivine oxide gabbro, then to subprismatic (and commonly foliated) ferrogabbro, and finally to granophyric monzodiorite. The more evolved and later emplaced components of the Beaver River diabase network are commonly distinguished as the Silver Bay intrusions in the southern Beaver Bay Complex (Fig. 1). Overall being intermediate in composition, the Silver Bay intrusions lithologies range from ophitic olivine gabbro to ferrogranite (Shank, 1989). Field mapping by Miller et al. (1994) found intrusive relationship between the Silver Bay intrusions and the Beaver River diabase. Angular inclusions of the host Beaver River diabase within marginal zones of the Silver Bay intrusions led Miller and Chandler (1997) to interpret that the Silver Bay intrusions intruded after the diabase crystallized.

One distinctive feature of the Beaver River diabase is its inclusions of anorthosite xenoliths. In the southern part of the Beaver Bay Complex, the Beaver River diabase occurs as dikes and sills, typically including anorthosites with various sizes ranging from centimeters to over 150 meters (Figs. 1, 3; Grout (1939); Morrison et al. (1983)). The diabase in this region intrudes the Palisade rhyolite of the North Shore Volcanic Group (Fig. 1), which has a $^{206}\text{Pb}/^{238}\text{U}$ date of $1093.94 \pm 0.28 \text{ Ma}$ (Swanson-Hysell et al., 2019). The Beaver River diabase is intruded by the Silver Bay intrusions here (Fig. 1). An aplite unit within the granophyre zone of one of these Silver Bay intrusions has a $^{206}\text{Pb}/^{238}\text{U}$

date of 1091.61 ± 0.14 Ma (Swanson-Hysell et al., 2019). Another arcuate, sill-like diabase body mapped as the Beaver River diabase outcrops along the eastern part of the complex (Fig. 1; Miller and Chandler (1997)). The diabase composition there is similar to that in the south and it also contains large anorthosite xenoliths that exceed 100 meters at Carlton Peak (Fig. 1). The Beaver River diabase in the northern part of the complex near the Houghtaling Creek area typically forms narrow, near-vertical dikes instead of sheets in the southern and eastern regions (Fig. 1; Miller et al. (1994)). The diabase in this region only locally contains xenoliths of anorthosite at dike margins.

Hundreds of anorthosite xenoliths have been recognized and mapped within the Beaver River diabase (Fig. 1). Many hill tops in the Beaver Bay Complex, such as the Carlton Peak and Britton Peak, are large anorthosite blocks (which lead Lawson (1893) to erroneously conclude that they were relict Archean topography). In the field, the anorthosites typically appear as subrounded to rounded, light-colored, translucent blocks that are in sharp contact with the hosting diabase (Fig. 3). They also occur as exposures whose contact with the diabase is covered (Fig. 3). Grout (1939) suggested that the rounded anorthosites are the result of friction during transportation as they were liberated by the diabase (i.e. physical weathering within a magmatic system). While the Beaver River diabase is chilled against the North Shore Volcanic Group lithologies that it intrudes, the diabase is not chilled against the margin of the anorthosite xenoliths (Morrison et al., 1983; Miller & Chandler, 1997). The lack of chilled contacts is consistent with the anorthosite being at elevated temperatures and cooling at the same time as the diabase magma.

The anorthosite xenoliths are dominantly monomineralic plagioclase that has an average anorthite content of $\sim 70\%$ (Morrison et al., 1983; Doyle, 2016). Interstitial pyroxene and olivine are present in minor concentrations in the xenoliths. Within the Carlton Peak anorthosite xenolith, up to 10 cm oikocrysts of altered mafic minerals such as olivine can occur. Nevertheless, the overall olivine content in the anorthosites is low. Interstitial titanomagnetite-ilmenite intergrowths that exceed $100 \mu\text{m}$ can be found through microscopy and $<20 \mu\text{m}$ Fe-Ti oxide grains can be detected with scanning electron microscopy (Fig. 3). Based on textural differences Morrison et al. (1983) divided the anorthosite xenoliths into four groups: one group which typically have well-developed granoblastic texture characterized by equigranular plagioclase crystals; another group which have interlocking, lath-shaped plagioclase crystals; an intermediate group which can have both

243 granoblastic texture and interlocking plagioclase laths; and a brecciated group that have
 244 brittle deformation textures superposed on pre-existing textures.

245 2.2 Portage Lake Volcanics and the Greenstone Flow

246 The Portage Lake Volcanics (PLV) is a ~5 km thick, normally magnetized, dom-
 247 inantly olivine basalt to andesite volcanic succession that outcrops in northern Michi-
 248 gan (particularly along the Keweenaw Peninsula) as well as on Isle Royale (Fig. 1, Huber
 249 (1973); Cannon and Nicholson (2001); Green (1982)). The Greenstone Flow of the Portage
 250 Lake Volcanic Group has been recognized as one of the largest lava flows on earth (Figs.
 251 1, 2). It outcrops as the main ridge along the Keweenaw Peninsula and Isle Royale (Fig.
 252 1). The flow can be correlated between the two outcrop regions on the basis of geochem-
 253 ical, petrographic and paleomagnetic similarity of the flow itself and the flows above and
 254 below (Longo, 1984). In both outcrop regions, the Greenstone Flow is underlain by con-
 255 glomerate and overlain by pyroclastic breccia (Lane, 1911; Huber, 1973). On the Keweenaw
 256 Peninsula, the Greenstone Flow is exposed over 90 km with a range of thickness from
 257 ~100 meters to a maximum thickness of over 450 meters, dipping to the northwest (Fig.
 258 1; White (1960)). On Isle Royale, the Greenstone Flow has a range of thickness from ~30
 259 meters to a maximum thickness of about 250 meters, dipping toward the southeast (Fig.
 260 1; Huber (1973)). More recently, Doyle (2016) estimated that the total aerial extent of
 261 the Greenstone Flow could be up to ~20000 km². Taking a range for this thickness of
 262 100 to 300 meters, Doyle (2016) estimated a total volume of 2000 to 6000 km³. This vol-
 263 ume range makes the Greenstone Flow one of the largest, if not the largest, single mafic
 264 lava flows on Earth (Fig. 2).

265 According to the mineralogical and textural attributes, Doyle (2016) divided the
 266 Greenstone Flow into four zones from bottom to top — lower ophitic zone, heterolithic
 267 zone, upper ophitic zone, and an amygdaloidal zone. Field observations, geochemical anal-
 268 yses and parent magma calculations conducted by Doyle (2016) suggest that the zoned
 269 Greenstone Flow formed through an open-system differentiation of a composite parent
 270 magma which is more evolved than the primitive olivine tholeiites generated by the Mid-
 271 continent Rift plume. That study proposed that the emplacement of the Greenstone Flow
 272 started with a voluminous eruption of olivine tholeiitic magma, forming the ophitic zones
 273 which subsequently inflated due to composite intrusions of more evolved basaltic magma
 274 which composes the heterolithic zone. A final stage of localized melt migration and dif-

275 differentiation resulted in the heterogeneous composition of the heterolithic zone. A $^{206}\text{Pb}/^{238}\text{U}$
 276 zircon date of 1091.59 ± 0.27 Ma for the Greenstone Flow was developed from a peg-
 277 matoid sample from the heterolithic zone (Swanson-Hysell et al., 2019).

278 3 Methods and Results

279 3.1 Zircon Geochronology and Geochemistry

280 A sample of an anorthosite xenolith within the Beaver River diabase was collected
 281 for U-Pb geochronology along Hwy 61 across from the Silver Bay taconite plant (MS99033;
 282 91.26358°W 47.28888°N ; Fig. 1). This sample comes from the same xenolith sampled for
 283 paleomagnetic study as site AX16 which has an exposed diameter of 27.5 meters (Fig.
 284 3). Thin sections were made from the geochronology sample as well as multiple paleo-
 285 magnetic cores. As is shown in Fig. 3F, plagioclase in this anorthosite xenolith have both
 286 equigranular crystals displaying a granoblastic texture and lath-shaped crystals display-
 287 ing an interlocking texture. The occurrence of both textures is consistent with an inter-
 288 pretation that this anorthosite xenolith formed under elevated temperatures and expe-
 289 rienced heating after initial crystallization.

290 Zircons were separated from a kilogram of the anorthosite using common mineral
 291 separation methods (Supporting Information). The separated zircons were subhedral to
 292 anhedral crystals (z1-z4) and platy fragments (z5-z8). The subhedral to anhedral crys-
 293 tals are consistent with intercumulus crystallization within an adcumulate with platy frag-
 294 ments also being a common zircon morphology within the Duluth Complex anorthositic
 295 series (e.g. samples AS-1 and FC-1 of Paces and Miller (1993)). Eight chemically-abraded
 296 zircons were analyzed by isotope dilution-thermal ionization mass spectrometry (ID-TIMS)
 297 in the Boise State Isotope Geology Laboratory using EARTHTIME tracer solutions (Condon
 298 et al., 2015). Both zircon morphologies yield indistinguishable dates. Using six of these
 299 single grain dates (and excluding two due to interpreted Pb-loss) results in a weighted
 300 mean $^{206}\text{Pb}/^{238}\text{U}$ date of $1091.83 \pm 0.21/0.37/1.15$ Ma (analytical/ analytical+tracer/
 301 analytical+tracer+decay uncertainty; Fig. 4).

302 This date provides a tight constraint on the age of the Beaver River diabase. Pre-
 303 viously, the maximum age constraint for the Beaver River diabase came from the rela-
 304 tionship that it cross-cuts the Palisade rhyolite of the North Shore Volcanic Group which
 305 has a $^{206}\text{Pb}/^{238}\text{U}$ date of 1093.94 ± 0.28 Ma (Swanson-Hysell et al., 2019). With this

new date, we know the crystallization age of the diabase to have been near-synchronous or younger with the date from the anorthosite xenolith. The Silver Bay intrusions, from which an aplite has a $^{206}\text{Pb}/^{238}\text{U}$ date of 1091.61 ± 0.14 Ma, (Fairchild et al., 2017), cross-cut the Beaver River diabase. These dates constrain the diabase to have been emplaced between 1091.83 ± 0.21 and 1091.61 ± 0.14 Ma (Fig. 4). Assuming a uniform probability of diabase emplacement between the aplite and anorthosite dates and their normal distributed uncertainties, a 95% confidence interval on the age of the diabase can be estimated by a Monte Carlo simulation (Supporting Information). This analysis gives an age for the diabase of 1091.7 ± 0.2 Ma (95% CI).

Using laser ablation-inductively coupled plasma mass spectrometry (LA-ICPMS), we collected geochemical trace element data from 15 additional zircons separated from sample MS90033 with both platy and subhedral to anhedral morphologies. Rare earth elements (REE) analyses from all zircons exhibit a significant negative Eu anomaly as opposed to the positive Eu anomaly in plagioclase from anorthosite xenoliths reported by Morrison et al. (1983) when normalized by Chondrite (Sun and McDonough (1989); Supporting Information). This result is consistent with the zircon crystallizing from the interstitial residual melt between the plagioclase crystals. In addition, the Ti-in-zircon thermometer records a range of zircon crystallization temperatures from 998°C to 860°C with a mean of $\sim 950^\circ\text{C}$ (Ferry and Watson (2007); Supporting Information).

3.2 Paleomagnetism

We sampled standard paleomagnetic cores along the southern and eastern Beaver Bay Complex with a particular focus on acquiring paired sites of anorthosite xenoliths and their local diabase hosts. Sample cores were collected using a hand-held gasoline-powered drill and were oriented using a magnetic compass as well as a sun compass when possible. Sun compass orientations were preferentially used for determining the sample azimuth. Typically, 7-10 cores were drilled for each anorthosite xenolith and their diabase hosts. A total of 17 diabase and 22 anorthosite sites were collected (Table 1). A table that summarizes the measured dimensions of each anorthosite xenolith sampled and the distance between each anorthosite paleomagnetic site and closest diabase host site is provided in the Supporting Information.

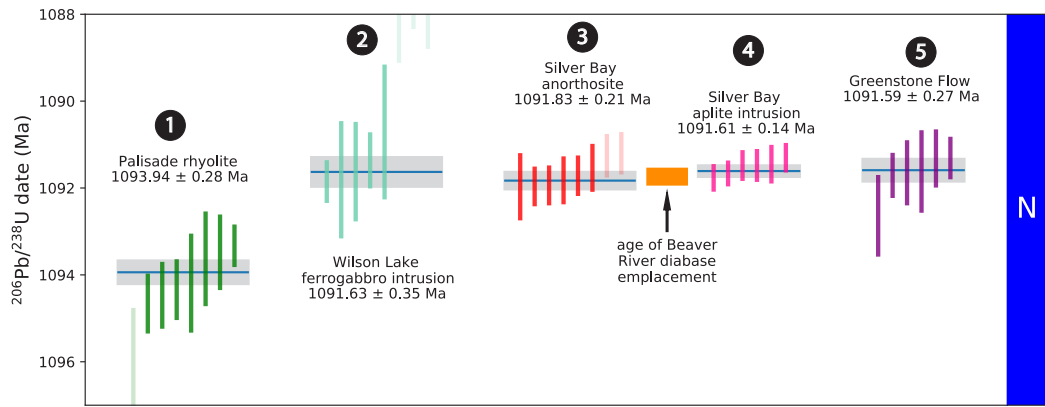


Figure 4: New $^{206}\text{Pb}/^{238}\text{U}$ zircon date of the anorthosite xenolith (dark orange) plotted in context of previously published $^{206}\text{Pb}/^{238}\text{U}$ zircon dates from the North Shore Volcanic Group (NSVG) and other Beaver Bay Complex intrusions (Swanson-Hysell et al., 2019, 2020). These high-precision dates are consistent with field observations that the Beaver River diabase crosscuts the Palisade rhyolite (dark green) and is cut by the Silver Bay intrusions (pink). Each vertical bar corresponds to one $^{206}\text{Pb}/^{238}\text{U}$ date from a single zircon crystal. The translucent bars represent zircons with interpreted Pb loss and are therefore not included in the weighted mean age calculations. Horizontal lines and gray boxes represent weighted mean $^{206}\text{Pb}/^{238}\text{U}$ dates and their analytical uncertainty. The numbers of each geochronology sample corresponds to those in Fig. 1 where locations of these samples are shown.

336 Samples underwent step-wise demagnetization and analyses in the magnetically shielded
 337 room in the UC Berkeley Paleomagnetism Lab. 7 sites from the Beaver River diabase
 338 underwent alternating field (AF) demagnetization with peak fields from 1 mT to 130 mT.
 339 An ASC TD-48SC thermal demagnetizer was used to demagnetize 10 diabase sites and
 340 all 22 anorthositic sites in a step-wise manner, with reduced step increments between 540°C
 341 and 585°C. The typical magnetic field inside the shielded room is <500 nT and the field
 342 inside the thermal demagnetizer chamber is <10 nT. The quartz glass sample rod of the
 343 UC Berkeley system is typically measured at 5×10^{-12} Am². All remanence measure-
 344 ments were made on a 2G Enterprises DC-SQUID superconducting rock magnetometer
 345 equipped with inline AF coils and an automated sample changer system. The PmagPy
 346 software package was used to implement least-square fits to specimen demagnetization
 347 data (Tauxe et al., 2016). Measurement level data are available within the MagIC database
 348 *for the purposes of review, these data are available in a pre-publication contribution within*
 349 *the MagIC database that can be accessed here: <https://earthref.org/MagIC/17102/400e0fb3-a79b-42bd-aeab-9005d2e3b438>*
 350

351 For both the diabase and anorthositic demagnetization, principal component anal-
 352 yses show that an origin trending characteristic remanent magnetization (ChRM) can
 353 be isolated after the removal of a minimal secondary component during the first few low
 354 coercivity (<10 mT) or low temperature (<200°C) demagnetization steps (Fig. 5). The
 355 ChRMs typically unblock through thermal demagnetization steps from ~500°C to ~580°C,
 356 consistent with them being held by low-titanium titanomagnetite. We interpret this com-
 357 ponent as a primary remanent magnetization acquired during the emplacement and cool-
 358 ing of the Beaver River diabase.

359 The site mean paleomagnetic directions are shown in Table 1. We present both AF
 360 and thermal demagnetization results for the Beaver River diabase as both methods are
 361 effective in removing the secondary components and isolating the coherent and univec-
 362 toral ChRM. Based on specimen and site level demagnetization behavior and the prox-
 363 imity between paired paleomagnetic sites of the anorthositic xenoliths and the diabase,
 364 we grouped the anorthositic xenoliths and their diabase hosts into individual cooling units
 365 and calculated a paleomagnetic pole position as the mean of the cooling unit virtual ge-
 366 omagnetic poles (Fig. 6).

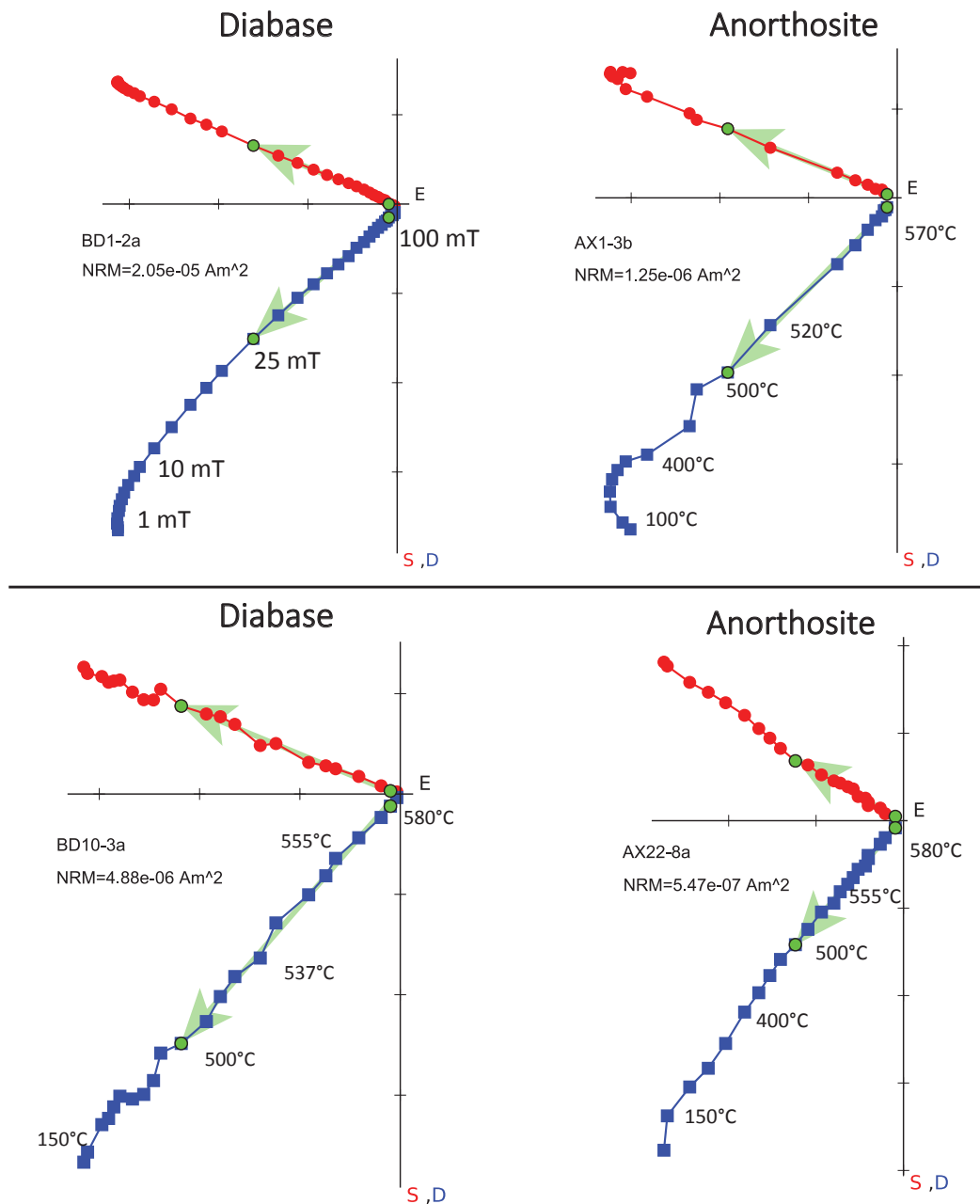


Figure 5: Example orthogonal vector demagnetization diagrams for diabase and anorthosite specimens. Anorthosite site AX1 is from a xenolith within the diabase sampled as BD1. Similarly, AX22 is from a xenolith with the BD10 diabase. Both AF and thermal demagnetization show dominantly univectoral decay of characteristic remanent magnetizations (ChRM) toward the origin after removal of minimal secondary components. The example specimen results show very similar ChRM directions between the paired diabase and anorthosite xenoliths sites.

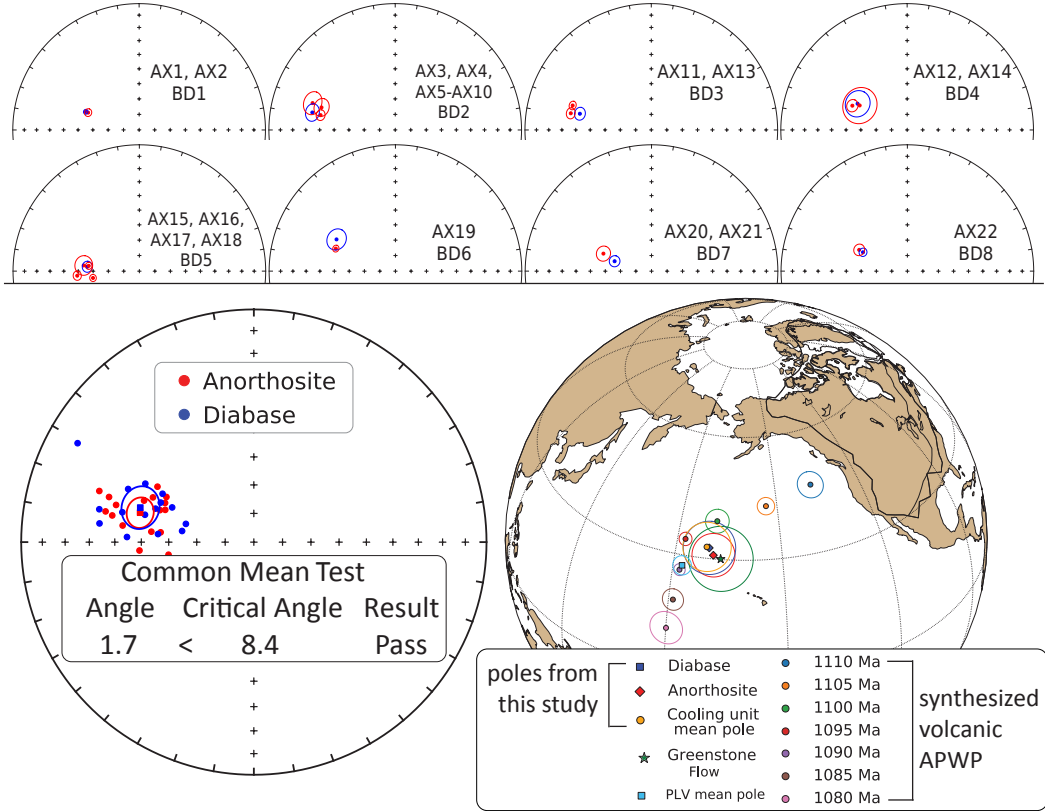


Figure 6: Top: Equal area plots of paleomagnetic directions from the anorthosite xenoliths and their local diabase hosts. AX: anorthosite xenolith site; BD: Beaver River diabase site. Bottom: Site mean paleomagnetic directions from the Beaver River diabase and anorthosite xenoliths are plotted on equal area plots. The anorthosite and diabase sites share a common mean as summarized by the results of the McFadden and McElhinny (1990) common mean test. Mean paleomagnetic pole positions of all diabase sites, all anorthosite sites, as well as a grand mean pole developed by grouping the anorthosite and diabase sites into individual cooling units are plotted against the synthesized Laurentia APWP based on poles from Midcontinent Rift volcanics and sedimentary rocks (Swanson-Hysell et al., 2019). The paleomagnetic poles from the diabase and anorthosite are indistinguishable with the Greenstone Flow pole developed by Foucher (2018), but they all are distinct from the Portage Lake Volcanics mean pole (Swanson-Hysell et al., 2019). All directions shown are tilt corrected.

Tilt-correcting the paleomagnetic directions to paleohorizontal is necessary for developing accurate paleomagnetic poles from the diabase and the anorthosite xenoliths to be compared to the Keweenawan Track apparent polar wander path (APWP; Fig. 6, Swanson-Hysell et al. (2019)). For intrusive igneous rocks, tilt corrections can be difficult to constrain due to the lack of paleohorizontal reference. Many paleomagnetic studies of Midcontinent Rift intrusive rocks in the Lake Superior region did not apply tilt corrections to their data (e.g., Beck & Lindsley, 1969; Beck, 1970; Books et al., 1966). However, we can determine the structural orientation of the Beaver River diabase using the abundant igneous fabric orientations measured on the diabase as well as bedding orientations measured from adjacent volcanic units (Boerboom, 2004; Boerboom & Green, 2006; Boerboom et al., 2006, 2007; Miller et al., 2001). We compile the igneous layering measurements from the Beaver River diabase and the volcanic bedding orientations from the Schroeder-Lutsen basalt which is overlying the Beaver Bay Complex. The mean tilt orientations of both units are similar (diabase dip direction - dip: 128.5 - 10.2; basalt dip direction - dip: 142.2 - 13.6). We combine the structural measurements from the Beaver River diabase and the Schroeder-Lutsen basalt and derived two sets of tilt corrections for the paleomagnetic directions of the diabase and anorthosite (dip direction - dip in the southern Beaver Bay complex: 128.7 - 12.9; in the eastern Beaver Bay Complex: 145.6-13.1, Supporting Information). The advantage of using the structural orientations from the Schroeder-Lutsen basalt is that the arcuate shape of the Beaver River diabase intrusions is nicely captured by the variation of lava dip directions while the dip angles of the basalt and diabase are very similar (Fig. 1).

The tilt-corrected ChRMs in both lithologies are northwest and down, yielding good specimen-level and site-level consistency (Fig. 5, 6). Close directional similarities between each anorthosite xenolith and their host diabase are supported by 9 out of a total of 17 diabase-anorthosite paleomagnetic site pairs passing a common mean test (McFadden & McElhinny, 1990). The overall mean directions between the two lithologies are indistinguishable as they also pass a common mean test (Fig. 6, McFadden and McElhinny (1990)). For the anorthosite sites that do not pass a common mean test with their diabase hosts, they nevertheless have coherent specimen-level directions that are very close to their host diabase directions (Fig. 6). We also plot the tilt-corrected mean pole of sites from both lithologies (diabase: 32.5°N, 189.5°E, N = 15, A95 = 6.3, k = 37.4; anorthosite: 30.9°N, 190.8°E, N = 17, A95: 5.2, k = 48.5) in context of a previously synthesized APWP

400 from the volcanics of the Midcontinent Rift (Swanson-Hysell et al., 2019) and show the
 401 poles to lie near the expected 1090 Ma and 1095 Ma pole positions (Fig. 6). The mean
 402 pole position of the interpreted cooling units (32.7°N , 188.8°E , $N = 15$, $A95 = 5.9$, $k =$
 403 41) lies close to the mean pole position derived from the *ca.* 1092 Ma Portage Lake Vol-
 404 canics (Fig. 6), consistent with the coeval magmatic activity between the Beaver River
 405 diabase and the Portage Lake Volcanics. This cooling unit mean pole paired with the
 406 estimated diabase emplacement age of 1091.7 ± 0.2 Ma is recommended to be used to
 407 as a paleomagnetic pole for the Beaver River diabase in future Laurentia Midcontinent
 408 Rift APWP compilations.

409 3.3 Thermal history model

410 The consistency of the paleomagnetic directions between the anorthosite xenoliths
 411 and the host diabase indicate that the anorthosites were heated above the Curie tem-
 412 perature of low-titanium titanomagnetite ($\sim 580^{\circ}\text{C}$) within the Beaver River diabase. To
 413 determine whether this thermal history is consistent with the geometry of the units and
 414 to gain more insight into the emplacement history of the xenoliths, we developed a cool-
 415 ing model. In this model, the anorthosite xenoliths are considered to be solid spheres
 416 with an initial cool temperature embedded in a uniform sheet of diabase magma (Delaney,
 417 1987; Unsworth & Duarte, 1979). The modeled thermal histories for various sizes of anorthosite
 418 xenoliths are shown in Fig. 7. In one end member case, the initial temperature of the
 419 anorthosites is assumed to be 50°C . While this temperature is unrealistically low given
 420 that the anorthosites likely have a deep crustal source, thermal modeling shows that even
 421 a 100-meter anorthosite xenolith with such low initial temperature would have been heated
 422 to the temperature of the tholeiitic magma (1150°C) within the sill. This temperature
 423 is well above the Curie temperature of magnetite. Anorthosite xenoliths with an assumed
 424 initial temperature of 500°C will equilibrate with the magma temperature on a similar,
 425 but slightly shorter, timescale. Therefore, the model predicts that the remanent mag-
 426 netizations of the anorthosites will be reset during emplacement within the diabase sills,
 427 regardless of their initial temperatures. Model parameters set to match the xenolith AX16,
 428 from which a U-Pb dates was developed in this study, leads to a model where the 27.5
 429 m xenolith would have stayed at the magma temperature for about 100 years after sill
 430 emplacement (Fig. 7). This duration estimate is a minimum as it does not consider heat-
 431 ing associated with melt in the lower crust or during ascent prior to emplacement. The

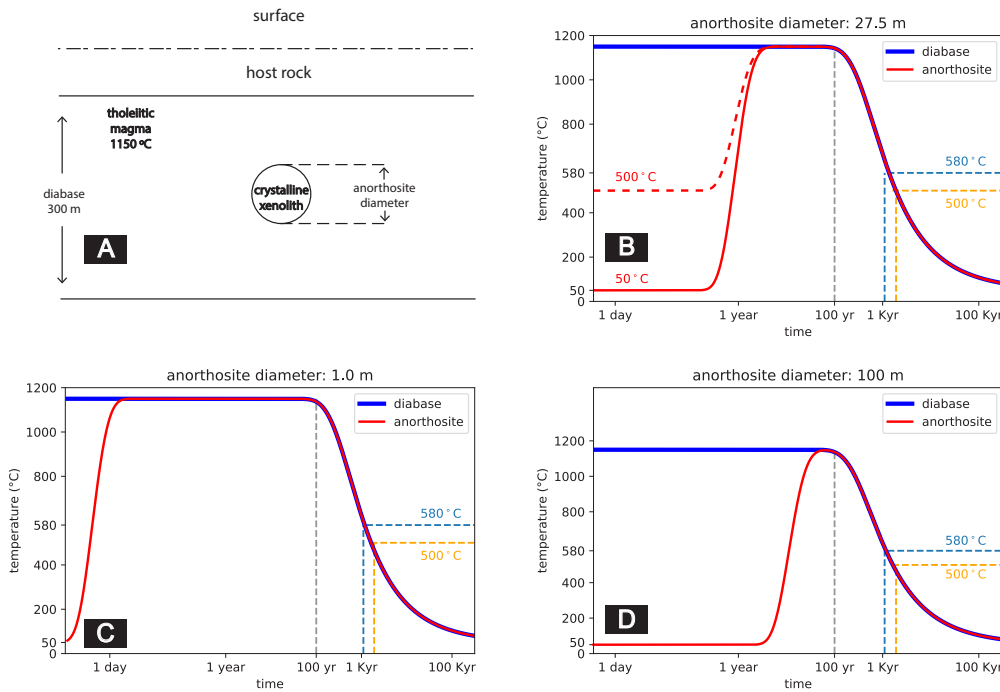


Figure 7: Thermal history model of the Beaver River diabase and its anorthosite xenoliths after emplacement at hypabyssal depths. (A) Schematic diagram for the thermal model considering cool anorthosite xenoliths as crystalline spheres residing in the middle of a diabase sill. Together they are hosted by cool country rocks at shallow depths. (B) Specific model for anorthosite AX16 (diameter of 27.5 meters) within its diabase sill host which is estimated to be 323 meters thick. (C) Thermal history model considering an anorthosite xenolith 1 meter in diameter residing in a 300 meter diabase sill. (D) Thermal history model considering an anorthosite xenolith 100 meter in diameter residing in a 300 meter diabase sill. These models show that anorthosite xenoliths were heated up to the diabase melt temperature after the emplacement, regardless of size. The time elapsed between at magnetite blocking temperatures (580°C and 500°C) during cooling is on the scale of a thousand years.

432 xenolith would have then cooled through the Curie temperature of magnetite (580°) af-
 433 ter ~ 1 kyr and acquired its magnetization as it cooled through magnetite blocking tem-
 434 peratures (down to $\sim 500^{\circ}$).

435 **4 Discussion**436 **4.1 Origin and Age of the Anorthosite Xenoliths**

437 The anorthosite xenoliths were liberated from depth and emplaced within the shal-
 438 low intrusions of the Beaver River diabase at 1091.7 ± 0.2 Ma (95% CI). This timing
 439 of emplacement is constrained by the Beaver River diabase postdating the new $^{206}\text{Pb}/^{238}\text{U}$
 440 zircon date of 1091.83 ± 0.21 Ma for the AX16 xenolith and being older than the cross-
 441 cutting 1091.61 ± 0.14 Ma Silver Bay intrusives.

442 The most straight-forward interpretation of the U-Pb dates is that the anorthosite
 443 xenoliths are entrained cumulates that crystallized just before the time of Beaver River
 444 diabase emplacement. This scenario would require that there were large lower crustal
 445 magma chambers in which flotation of plagioclase resulted in cumulate formation both
 446 during *ca.* 1092 Ma Beaver Bay Complex magmatism and *ca.* 1096 Ma Duluth Com-
 447 plex magmatism. We know that during Duluth Complex time, conditions existed for an
 448 anorthosite-generating, deep-crustal magma chamber that resulted in the emplacement
 449 of one of the largest layered mafic intrusions on Earth. The Duluth Complex also con-
 450 tains anorthosite xenoliths within gabbroic anorthosite of the Anorthositic Series (Fig.
 451 9, Miller and Weiblen (1990)). Both the crystal-rich magma that formed the Duluth Com-
 452 plex Anorthositic Series and more crystal-poor magmas of the Duluth Complex Layered
 453 Series were rapidly emplaced within < 500 kyr, between 1096.19 ± 0.19 Ma and 1095.69
 454 ± 0.18 Ma ($^{206}\text{Pb}/^{238}\text{U}$ ages, Swanson-Hysell et al. (2020)), about 4 myr before the em-
 455 placement of the Beaver River diabase. Given the known anorthosite generation during
 456 Duluth Complex magmatism, it is worth considering whether it is reconcilable with the
 457 data for the anorthosite cumulates xenoliths to have crystallized *ca.* 1096 Ma, but give
 458 U-Pb zircon dates of *ca.* 1091.8 Ma.

459 The significant negative Eu anomaly in the zircons within the anorthosite constrains
 460 them to have crystallized from a magma that had experienced significant plagioclase ex-
 461 traction (Rubatto (2002); Schaltegger et al. (1999); Supporting Information). This re-
 462 sult indicates that the zircons were comagmatic with their host anorthosite plagioclase.
 463 The Ti-in-zircon temperature estimates indicate that they crystallized from temperatures
 464 of 998 to 860°C (Ferry & Watson, 2007). In addition, zircons that have lower Ti-in-zircon
 465 temperatures have lower Eu abundance, but enrichment of incompatible elements such
 466 as Hf and Th (Supporting Information). This systematic pattern of elemental concen-

tration variation is consistent with the zircons crystallizing from residual melts on a cooling path that increased incorporation of incompatible trace elements and deepened the Eu anomaly with decreasing temperature and melt fraction. Scanning electron microscopy on two undated anorthosite xenoliths with plagioclase laths displaying interlocking textures reveals zircon crystals with subhedral to anhedral shapes within the mineral assemblage that is interstitial to the plagioclase (Supporting Information). Cathodoluminescence (CL) images show internal zoning in zircons which can be attributed to variations in REE, particularly Dy elemental concentrations, during zircon crystallization (Remond et al. (1992); Supporting Information). These data confirm that the zircons formed from residual melt within the interstitial spaces of the plagioclase cumulate and are inconsistent with a later metamorphic origin.

Zircon U-Pb dates nearly always record crystallization age of their host rock, as the zircon crystallization temperature is similar to that of the host rock. However, the anorthosites are a rather unique case given that the melting point of anhydrous plagioclase with an average composition of the Beaver River anorthosite (~70% anorthite, Morrison et al. (1983); Doyle (2016)) is ~1400°C. Thermal history modeling indicates that the xenoliths would have equilibrated to the temperature of the olivine tholeiitic magma (~1100 to 1200°C) and remained at that temperature for more than 100 years in the diabase sill interior (Fig. 7). While these temperatures would not have melted the plagioclase or zircon, these temperatures are high enough for there to start to be appreciable Pb diffusion out of zircon. However, the magnitude of Pb diffusion is dependent on the time spent at such a temperature. If a temperature of 1200°C is sustained for ~10 thousand years (longer than the modeled time), ~90% of Pb will diffuse out of a ~120 μm diameter zircon (Cherniak & Watson, 2001). Zircons that crystallized at 1096 Ma and then lost >90% of their Pb at 1091.6 Ma could give apparent U-Pb dates of 1091.8 Ma (Supporting Information). However, CL imagery reveals sharp boundaries between zones of differing CL response (Supporting Information) on the scale of ~2 μm . Such CL zoning patterns are dominantly attributed to the Dy concentration variations (Remond et al., 1992). A time-temperature history that results in 90% Pb diffusion out of a 120 μm diameter zircon would also cause Dy re-equilibration throughout a zircon, leaving no clear zonation. Therefore a scenario where the zircons first crystallized during Duluth Complex magmatism and subsequently lost more than 90% of Pb is difficult to reconcile with the preservation of such thin zonations.

500 Based on Sm-Nd isotopic data, Morrison et al. (1983) favored a scenario where the
501 anorthosite cumulates became xenoliths at an age of 1.9 Ga. While a ca. 1096 Ma Duluth
502 Complex age is difficult to explain given the U-Pb dates, a ca. 1900 Ma age can-
503 not be reconciled with the data. To reset the U-Pb date of the zircons to be 1091.8 Ma
504 at an emplacement time of 1091.6 Ma (the minimum age of emplacement for the Silver
505 Bay intrusion date, Fig. 4) would require diffusive loss of >99.95% of the Pb from the
506 zircons (Supporting Information). More Pb retention in zircons will exhibit as signifi-
507 cant discordant ages and be inconsistent with the geochronology data (Fig. 4). The Sm-
508 Nd age of 1.9 Ga from the anorthosite xenoliths is more likely the result of contamina-
509 tion by older crust. Isotopic studies of MCR felsic rocks by Vervoort et al. (2007) indi-
510 cate that anatetic melts in the early MCR magmatic stage were largely generated from
511 Early Proterozoic (~2.1 Ga) crust. Because of assimilation and anatexis of the lower crust,
512 the plagioclase cumulates where the anorthosite xenoliths originated could have recorded
513 this contamination, which is eventually reflected in the older Sm-Nd isotopic signatures
514 within the Beaver River anorthosite xenoliths discovered by Morrison et al. (1983).

515 An alternative scenario consistent with an older formation age of the anorthosites
516 is if the zircons crystallized long after the plagioclase. This scenario would require that
517 interstitial melt pockets from which zircons crystallized remained liquid within the pla-
518 gioclase cumulate until they were entrained by the Beaver River diabase *ca.* 1092 Ma
519 and cooled. The mantle plume related heat regime of the Yellowstone hotspot has led
520 to modern Moho temperatures that can be >800°C (Schutt et al., 2018) . If a similar
521 heat regime occurred during the crystallization of the anorthositic mush of the Duluth
522 Complex magmatism and was sustained for 4 millions of years, there is the potential for
523 partial melt. However, it would be difficult for such melt to stay in place and not to dif-
524 fuse out of the cumulate on these long timescales.

525 The geochemical evidence for the zircons being comagmatic with the plagioclase
526 is difficult to reconcile with zircon crystallization significantly postdating anorthosite cu-
527 mulate formation. The presence of REE zonation is difficult to reconcile with scenarios
528 where there is significant Pb diffusion that appreciably reset the U-Pb dates. It is likely
529 that Beaver River diabase anorthosite xenoliths are entrained cumulate enclaves of Beaver
530 Bay Complex magmatism. Regardless, the U-Pb date of 1091.83 ± 0.21 Ma from zir-
531 cons in the anorthosite xenolith constrains the Beaver River diabase to have been em-

532 placed after that date and before the 1091.61 ± 0.14 Ma date of the cross-cutting Sil-
 533 ver Bay aplite intrusion (Fig. 4).

534

4.2 A comagmatic relationship between the Beaver River diabase and 535 the Greenstone Flow

536 Given the existence of many anorthosite xenoliths whose short-axis diameters of-
 537 ten reach tens of meters and can be as wide as 180 meters (Fig. 1; Boerboom (2004);
 538 Boerboom et al. (2006)), the Beaver River diabase magma conduits must have been at
 539 least this wide during magma ascent. It would be consistent with such wide conduits ex-
 540 tending to hypabyssal depths for magma that flowed through these conduits to have vented
 541 to the surface.

542 The high volume and composite nature of the extrusive Greenstone Flow of the Portage
 543 Lake Volcanics lead to a match for this large and composite feeder system. Doyle (2016)
 544 proposed a comagmatic link between the Beaver River diabase and the Greenstone Flow.
 545 Doyle (2016) discovered that both the intrusive diabase and the extrusive volcanics have
 546 almost indistinguishable primary compositions that followed similar differentiation pat-
 547 terns. Doyle (2016) also points to a shared petrographic textures between the ophitic
 548 Beaver River diabase and the ophitic Greenstone Flow, which features the plagioclase
 549 laths clustering together and joining along their long crystallographic axes. The fosterite
 550 content of the olivines and enstatite content of the pyroxenes in the Beaver River dia-
 551 base together with the Silver Bay intrusions, and the Greenstone Flow have overlapping
 552 compositions consistent with a same magma (Fig. 8). The composition of the plago-
 553 clase within the units further strengthens this interpretation. Although there are no known
 554 multi-crystalline anorthosite xenoliths in the Greenstone Flow, plagioclase megacrysts
 555 occur in the lava flow. Analyses of the anorthite content from plagioclase megacrysts show
 556 very similar values between the Beaver River diabase and the Greenstone Flow basalt
 557 (Fig. 8, Doyle (2016)). In both units, the plagioclase cores are more enriched in anor-
 558 thite than the rim and the groundmass. These data provide evidence that the core of
 559 the plagioclase megacrysts in the Greenstone Flow derived from a similar source with
 560 those in the Beaver River diabase and that the rims are later overgrowths. These min-
 561 eralogical similarities are consistent with the interpretation that the Beaver River dia-
 562 base and the Greenstone Flow have the same magma source.

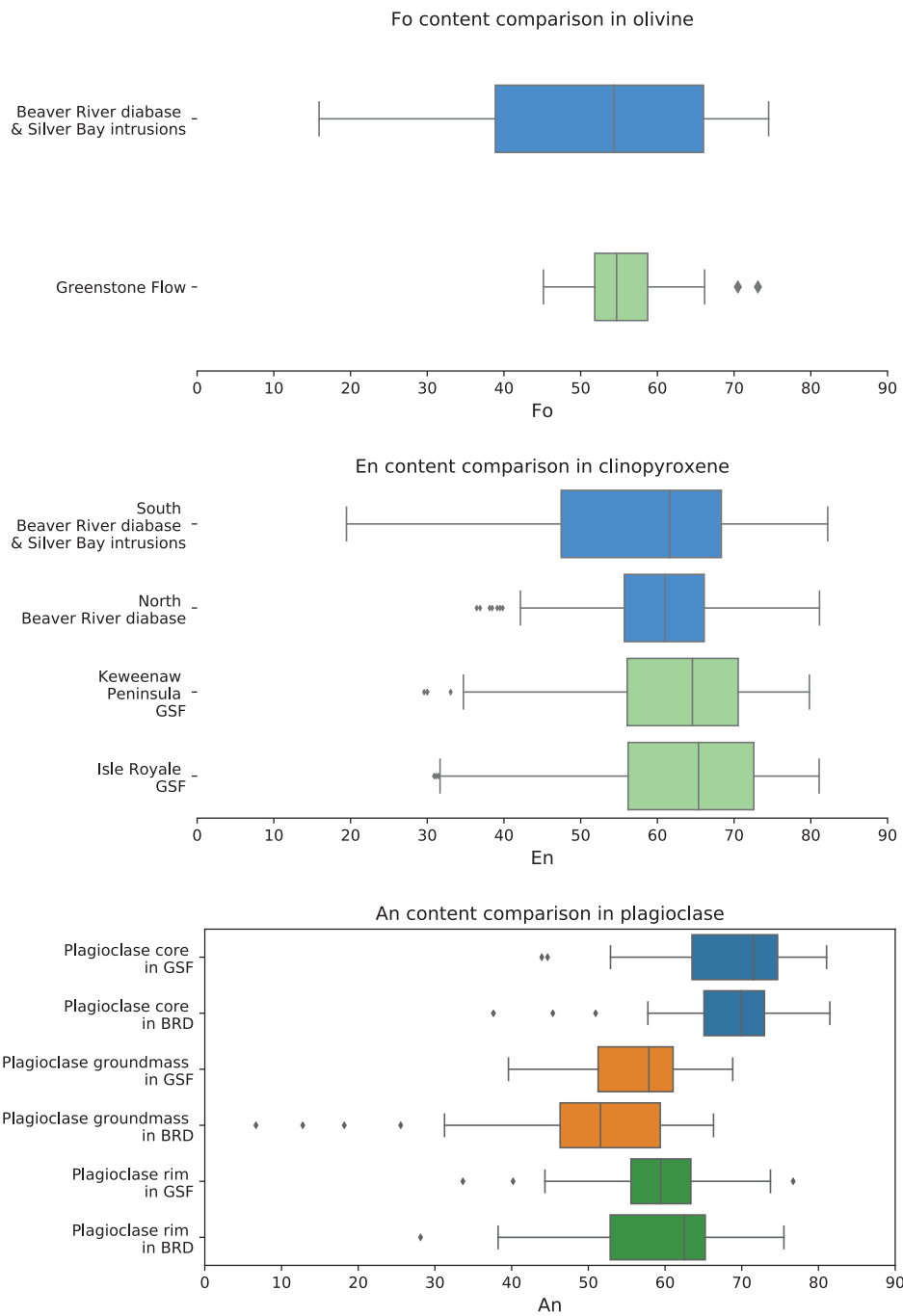


Figure 8: Box plots of geochemical analyses of olivine, pyroxene, and plagioclase in the Beaver River diabase (BRD) and Greenstone Flow (GSF). The fosterite content in olivine crystals and the enstatite content in clinopyroxene crystals are very similar in the Beaver River diabase and the Greenstone Flow. The anorthite concentrations in the core, groundmass, and rim of the plagioclase megacrysts within the Beaver River diabase and the Greenstone Flow share very similar patterns and the distributions are nearly identical. The box encloses the middle 50% of the data ranges (i.e., the interquartile range), and the notch represents the median values. The whiskers extend to the 2.5th and 97.5th percentile values. Fo-fosterite; En-enstatite; An-anorthite. Data from Doyle (2016).

The magmatic linkage between the Beaver River diabase and the Greenstone Flow inferred from comparable lithologies and geochemistry can be further evaluated using the paleomagnetic pole positions and radiometric dates from both units (Fig. 6, 4). The heat diffusion model of the cooling history of the anorthosite xenoliths within the diabase suggests that the time it takes to cool the diabase and anorthosite from low-titanium titanomagnetite Curie temperature ($\sim 580^{\circ}\text{C}$) to their blocking temperatures ($\sim 500^{\circ}\text{C}$) is on the time scale of a few thousand years (Fig. 7). This time scale is close to the typical 10^4 years which is considered to be sufficient for averaging out secular variations of the geomagnetic field. Fig. 6 shows the site mean paleomagnetic pole positions from all diabase and anorthosite sites in this study against the previously synthesized Laurentia APWP developed using an Euler pole inversion to chronostratigraphically constrained volcanic poles in present-day coordinates (Swanson-Hysell et al., 2019). The site-mean pole positions of the diabase and anorthosite overlap within uncertainty ellipses and the mean pole positions fall between the 1095 Ma and 1090 Ma pole path positions (Fig. 6), consistent with the geochronology results (Fig. 4). Further, the mean paleomagnetic pole position derived from the Greenstone Flow share a common mean with those of the Beaver River diabase and the anorthosite xenoliths, but none of these poles share a common mean with the mean pole derived from the Portage Lake Volcanics (Fig. 6; Swanson-Hysell et al. (2019)). This result suggests that the timescale over which the Beaver River diabase and the Greenstone Flow acquired their magnetization may be too short to fully average out secular variation. In this case, the overlapping pole positions between the Beaver River diabase and the Greenstone Flow strengthens their temporal correlation even more (Fig. 6).

The U-Pb dates provide strong support for this hypothesis by revealing coincident ages for the Beaver River diabase and the Greenstone Flow. The age of the Beaver River diabase is constrained to be between the $^{206}\text{Pb}/^{238}\text{U}$ dates of 1091.83 ± 0.21 Ma and 1091.61 ± 0.14 Ma (Fig. 4) giving an age estimate of 1091.7 ± 0.2 Ma (95% CI). This age is indistinguishable with the $^{206}\text{Pb}/^{238}\text{U}$ date of 1091.59 ± 0.27 Ma for the Greenstone Flow (Fig. 4). These chronological constraints are consistent with a comagmatic linkage between the Beaver River diabase and the Silver Bay intrusions and the extrusive Greenstone Flow.

The Portage Lake Volcanics, including the Greenstone Flow, are interpreted to have erupted into the main central graben of the Midcontinent Rift during an interval of sig-

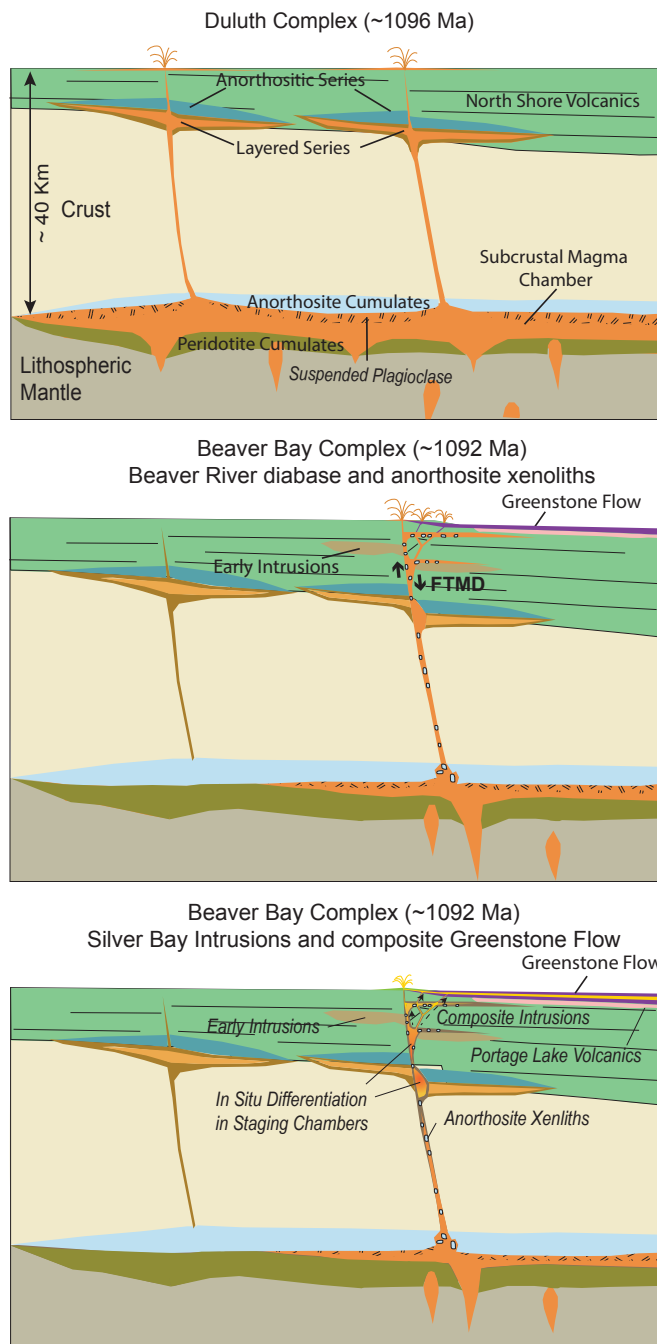


Figure 9: Schematic model for the emplacement of the *ca.* 1096 Ma Duluth Complex, the *ca.* 1092 Ma Beaver Bay Complex, Greenstone Flow and associated anorthositic lithologies. Top: Duluth Complex Anorthositic Series formed by subhorizontal emplacement of plagioclase crystal mushes generated by plagioclase flotation in subcrustal magma chambers. The Layered Series formed by emplacement of crystal-poor mafic magmas beneath the Anorthositic Series and variable differentiation by in situ fractional crystallization. Middle: Intrusion of the anorthosite xenolith-bearing Beaver River diabase of the Beaver Bay Complex along a major crustal fault (FTMD-Finland Tectonomagnetic Discontinuity) and its massive eruption at surface to form the Greenstone Flow. Bottom: Emplacement of the composite Beaver River diabase and Silver Bay intrusions into the diabase and the Greenstone Flow were generated by differentiation in deeper staging chambers. The erosional unconformity between the Schroeder-Lutsen basalt and the Beaver River diabase suggest the diabase was emplaced into an uplifted rift flank highland, allowing for flank eruptions of the Greenstone Flow and other Portage Lake Volcanics into the main Midcontinent Rift basin.

nificant subsidence (Fig. 9; Miller and Chandler (1997); Cannon and Hinze (1992)). In contrast to the thick accumulation in the Portage Lake Volcanics, the Beaver Bay Complex has an erosional (and slightly angular) unconformity atop it that is then covered by the the younger Schroeder-Lutsen basalt (Fig. 1; Miller et al. (2001)). This relationship suggests that the Beaver River diabase was emplaced into a rift flank highland that experienced uplift during the active development of the central graben (Swanson-Hysell et al., 2019). Eruptions fed through the Beaver River diabase network could have emerged from the rift flank or flowed from the highland into main rift basin where it accumulated as the Greenstone Flow and associated Portage lake Volcanics (Fig. 9). Silver Bay intrusions from chambers of differentiated staging magmas later intruded the Beaver River diabase and the Greenstone Flow, adding to the composite lithologies of the lava flow and further inflating its heterolithic zone (Fig. 9). If the Greenstone Flow indeed connects through the Lake Superior basin to NE Minnesota and the Beaver River diabase, the volume of $\sim 1650 \text{ km}^3$ estimated by Longo (1984) must be a minimum. The full volume of the Greenstone Flow likely reaches $\sim 6000 \text{ km}^3$ (Doyle, 2016), rivaling the largest known lava flows on Earth (Fig. 2).

5 Conclusion

High-precision U-Pb dates, together with paleomagnetic data, support the hypothesis that the Beaver River diabase was a feeder system to the high-volume Greenstone Flow. This intrusive-extrusive linkage is further bolstered by the similar compositions of the units. The large anorthosite xenoliths within the Beaver River diabase require that conduits feeding the magma to the surface had diameters that exceeded 150 meters. As a result, there was voluminous emplacement of magma into the shallow subsurface and eruption into the Midcontinent Rift basin *ca.* 1092.7 Ma at the end of the main stage of Midcontinent Rift magmatism.

Acknowledgments

This research was funded by NSF EAR-1847277 to N.L.S.-H. and an Institute on Lake Superior Geology Student Research Fund grant to Y.Z. Permits for fieldwork and sampling from the Minnesota Department of Natural Resources are gratefully acknowledged. We thank James Pierce and Blake Hodgin for assistance in the field. We thank Stephen Self for providing constructive comments regarding mafic lava flow volumes. We thank

627 John Grimsich and Tim Teague at UC Berkeley EPS department for their help with pet-
628 rographic sample preparation and analyses. Paleomagnetic data associated with this study
629 are available within the MagIC database (<https://earthref.org/MagIC/17089/26d9073f-2447-4f46-85fb-8596ce5b3aab>) and all data are within a Github repository associ-
630 ated with this work (https://github.com/Swanson-Hysell-Group/2021_AX_BD) that
631 is also archived on Zenodo (insert URL after revisions). This repository also contains
632 Python code related to calculations, visualizations and statistical tests discussed herein.
633

Table 1:
Summary of new site level paleomagnetic data for the Beaver River diabase and anorthosite xenoliths. n/N: number of samples/sites analyzed and included in the site/grand mean; dec_{is} & inc_{is} : in situ mean declination and inclination for the site; dec_{te} & inc_{te} : tilt-corrected mean declination and inclination for the site; k: Fisher precision parameter; R: resultant vector length; α_{95} : 95% confidence limit in degrees; VGP lat.—latitude of the virtual geomagnetic pole for the site; VGP lon—longitude of the virtual geomagnetic pole for the site. Full measurement level data are available within the MagIC database. <https://earthref.org/MagIC/17102/400e0fb3-a79b-42bd-aaeb-9005d2a3b488>.

site	lat	lon	n/N	dec_{is}	dec_{te}	inc_{is}	inc_{te}	k	α_{95}	VGP lat _{is}	VGP lon _{is}	VGP lat _{te}	VGP lon _{te}
AX1	47.2	-91.4	8.0	293.3	42.6	288.8	54.9	536.0	2.4	33.4	180.0	37.1	193.2
AX2	47.2	-91.4	9.0	282.0	31.3	277.4	42.6	145.0	4.3	20.4	181.8	22.6	191.1
AX3	47.6	-90.9	10.0	290.4	28.2	285.1	38.6	69.0	5.9	24.7	174.5	25.9	183.7
AX4	47.6	-90.9	7.0	291.9	20.0	288.3	30.7	91.0	6.4	22.3	169.8	24.4	177.2
AX5-10	47.6	-90.9	14.0	286.2	29.1	280.7	38.1	269.5	2.5	22.3	178.1	22.7	186.5
AX11	47.4	-91.2	8.0	284.9	23.5	281.7	35.2	305.0	3.2	19.1	176.3	22.0	184.1
AX12	47.3	-91.3	6.0	299.9	42.5	297.3	55.2	36.0	11.3	37.8	175.1	43.0	188.4
AX13	47.4	-91.2	9.0	289.8	23.0	287.3	35.1	434.0	2.5	22.2	172.4	25.7	180.0
AX14	47.3	-91.3	7.0	296.9	38.2	293.9	50.8	256.0	3.8	33.7	174.5	38.2	186.1
AX15	47.3	-91.3	8.0	282.9	42.3	275.8	53.5	86.0	6.0	26.2	187.2	27.9	199.8
AX16	47.3	-91.3	8.0	273.7	39.1	265.8	49.2	396.0	2.8	18.5	191.6	19.0	202.9
AX17	47.3	-91.3	8.0	273.6	49.8	261.6	59.6	647.0	2.2	24.3	198.3	23.7	213.5
AX18	47.3	-91.3	9.0	283.8	45.5	276.0	56.9	535.0	2.2	28.5	188.7	30.2	202.8
AX19	47.3	-91.3	8.0	293.9	35.8	290.7	48.2	65.0	2.1	30.5	175.4	34.6	186.0
AX20	47.3	-91.3	5.0	294.5	44.3	290.0	56.7	271.0	4.7	35.1	180.4	39.0	194.5
AX21	47.3	-91.3	8.0	301.7	37.7	301.7	50.5	803.0	2.0	36.7	170.4	42.1	181.7
AX22	47.4	-91.2	9.0	297.2	43.1	293.8	55.7	208.0	3.6	36.3	177.6	41.0	191.1
Anorthosite mean		17.0	289.3	36.5	284.5	48.2	55.0	4.9	28.0	179.6	30.9	190.8	
BD1	47.2	-91.4	15.0	293.1	40.9	288.8	53.2	623.0	1.5	32.4	179.0	36.1	191.6
BD2	47.6	-90.9	8.0	286.6	22.7	282.0	32.6	122.0	5.0	19.9	175.0	21.0	182.8
BD3	47.4	-91.2	8.0	286.6	29.8	282.8	41.6	212.0	3.8	22.9	177.9	25.8	186.9
BD4	47.3	-91.3	8.0	300.2	40.7	297.9	53.4	47.0	8.2	37.1	173.6	42.3	186.0
BD5	47.3	-91.3	8.0	282.7	44.8	274.8	56.0	271.0	3.4	27.4	188.9	28.9	202.6
BD6	47.3	-91.3	9.0	300.0	33.2	298.3	64.0	64.0	6.5	33.4	169.2	38.6	178.9
BD7	47.3	-91.3	7.0	292.4	53.1	285.0	65.3	305.0	3.5	38.5	189.2	41.3	208.3
BD8	47.2	-91.4	10.0	287.9	52.8	278.8	64.5	300.0	2.8	35.3	191.8	37.1	209.9
BD9	47.2	-91.3	7.0	278.2	33.8	272.3	44.6	55.0	8.2	19.0	185.7	20.4	195.6
BD10	47.4	-91.2	10.0	297.0	46.2	293.0	58.7	341.0	2.6	37.8	180.0	42.2	195.1
BD11	47.4	-91.3	8.0	296.4	41.7	293.0	54.2	429.0	2.7	35.1	177.1	39.5	189.9
BD12	47.3	-91.3	8.0	288.8	38.1	284.1	50.1	141.0	4.7	28.1	180.4	31.3	191.8
BD13	47.5	-91.1	8.0	280.4	22.4	276.9	33.6	341.0	3.0	15.6	179.2	18.0	186.7
BD15	47.7	-90.6	8.0	300.1	2.3	299.3	14.2	119.0	5.1	20.6	156.9	24.8	161.7
BD17	47.4	-91.2	8.0	295.1	28.5	292.9	41.0	550.0	2.4	28.0	170.8	32.3	179.3
Diabase mean		15.0	291.0	35.7	286.9	47.7	51.6	5.0	29.0	178.2	32.5	189.5	

634 **References**

- 635 Beck, M. E. (1970). Paleomagnetism of Keweenawan Intrusive Rocks, Minnesota. *Journal of Geophysical Research*, 75(26), 4985–4996. doi: 10.1029/jb075i026p04985
- 636 Beck, M. E., & Lindsley, N. C. (1969). Paleomagnetism of the Beaver Bay Complex, Minnesota. *Journal of Geophysical Research*, 74(8), 2002–2013. doi: 10.1029/jb074i008p02002
- 638 Boerboom, T. J. (2004). *M-147 Bedrock geology of the Split Rock Point quadrangle, Lake County, Minnesota* (Tech. Rep.). Minnesota Geological Survey.
- 639 Boerboom, T. J., Green, J., & Albers, P. (2007). *M-174 Bedrock geology of the Lutzen quadrangle, Cook County, Minnesota* (Tech. Rep.). Minnesota Geological Survey.
- 640 Boerboom, T. J., & Green, J. C. (2006). *M-170 Bedrock geology of the Schroeder quadrangle, Cook County, Minnesota* (Tech. Rep.). Minnesota Geological Survey.
- 641 Boerboom, T. J., Green, J. C., Albers, P., & Miller, J., J.D. (2006). *M-171 Bedrock geology of the Tofte quadrangle, Cook County, Minnesota* (Tech. Rep.). Minnesota Geological Survey.
- 642 Books, K. G., White, W. S., & Beck, M. E. (1966). *Magnetization of Keweenawan gabbro in northern Wisconsin and its relation to time of intrusion*. Geological Survey Research.
- 643 Bryan, S. E., Peate, I. U., Peate, D. W., Self, S., Jerram, D. A., Mawby, M. R., ... Miller, J. A. (2010). The largest volcanic eruptions on Earth. *Earth-Science Reviews*, 102(3-4), 207–229. doi: 10.1016/j.earscirev.2010.07.001
- 644 Cannon, W. F., & Hinze, W. J. (1992). Speculations on the origin of the North American Midcontinent rift. *Tectonophysics*, 213(1-2), 49–55. doi: 10.1016/0040-1951(92)90251-z
- 645 Cannon, W. F., & Nicholson, S. W. (2001). Geologic map of the Keweenaw Peninsula and adjacent area, Michigan. *USGS Numbered Series*, 2696.
- 646 Cherniak, D., & Watson, E. (2001). Pb diffusion in zircon. *Chemical Geology*, 172(1-2), 5–24. doi: 10.1016/s0009-2541(00)00233-3
- 647 Condon, D. J., Schoene, B., McLean, N. M., Bowring, S. A., & Parrish, R. R. (2015, 9 1). Metrology and traceability of U-Pb isotope dilution geochronology

- 667 (EARTHTIME tracer calibration part I). *Geochimica et Cosmochimica Acta*,
668 *164*, 464–480. doi: 10.1016/j.gca.2015.05.026
- 669 Davis, D. W., & Paces, J. B. (1990). Time resolution of geologic events on the
670 Keweenaw Peninsula and implications for development of the Midcontinent
671 Rift system. *Earth and Planetary Science Letters*, *97*(1-2), 54–64. doi:
672 10.1016/0012-821x(90)90098-i
- 673 Delaney, P. (1987). *Heat transfer during emplacement and cooling of mafic dykes*.
674 Geological Association of Canada.
- 675 Doyle, M. (2016). *Geologic and geochemical attributes of the Beaver River Diabase*
676 *and Greenstone Flow: Testing a possible intrusive-volcanic link in the 1.1 Ga*
677 *Midcontinent Rift* (Unpublished master's thesis). University of Minnesota.
- 678 Fairchild, L. M., Swanson-Hysell, N. L., Ramezani, J., Sprain, C. J., & Bowring,
679 S. A. (2017). The end of Midcontinent Rift magmatism and the paleogeogra-
680 phy of Laurentia. *Lithosphere*, *9*(1), 117–133. doi: 10.1130/l580.1
- 681 Ferry, J. M., & Watson, E. B. (2007). New thermodynamic models and revised cal-
682ibrations for the Ti-in-zircon and Zr-in-rutile thermometers. *Contributions to*
683 *Mineralogy and Petrology*, *154*(4), 429–437. doi: 10.1007/s00410-007-0201-0
- 684 Foucher, M. (2018). *Probing the Precambrian geodynamo: analysis of the geomag-*
685 *netic field behavior and calibration of pseudo-thellier paleointensity method for*
686 *Mesoproterozoic rocks* (Unpublished doctoral dissertation). Michigan Techno-
687 logical University.
- 688 Green, J. C. (1982). 5: Geology of Keweenawan extrusive rocks. *Geological Society*
689 *of America Memoirs*, *156*, 47–56.
- 690 Grout, S. G. M., Frank F. (1939). The geology of the anorthosites of the Minnesota
691 coast of Lake Superior. Minnesota Geological Survey.
- 692 Heaman, L. M., Easton, R. M., Hart, T. R., Hollings, P., MacDonald, C. A., &
693 Smyk, M. (2007). Further refinement to the timing of Mesoproterozoic mag-
694 matism, Lake Nipigon region, Ontario. *Canadian Journal of Earth Sciences*,
695 *44*(8), 1055–1086. doi: 10.1139/e06-117
- 696 Hinze, W. J., & Chandler, V. W. (2020). Reviewing the configuration and extent
697 of the Midcontinent Rift system. *Precambrian Research*, *342*, 105688. doi: 10
698 .1016/j.precamres.2020.105688
- 699 Huber, N. (1973). *The Portage Lake Volcanics (Middle Keweenawan) on Isle*

- Ga Midcontinent Rift in the Lake Superior Region – An Overview. In *Field guide to the copper-nickel-platinum group element deposits of the lake superior region*. Precambrian Research Center.

Miller, J., J.D., Severson, M. J., Chandler, V. W., & Peterson, D. M. (2001). *M-119 Geologic map of the Duluth Complex and related rocks, northeastern Minnesota* (Tech. Rep.). Minnesota Geological Survey.

Miller, J., J.D., & Weiblen, P. W. (1990). Anorthositic rocks of the Duluth Complex: Examples of rocks formed from plagioclase crystal mush. *Journal of Petrology*, 31(2), 295–339. doi: 10.1093/petrology/31.2.295

Morrison, D. A., Ashwal, L. D., Phinney, W. C., Shih, C.-Y., & Wooden, J. L. (1983). Pre-Keweenawan anorthosite inclusions in the Keweenawan Beaver Bay and Duluth Complexes, northeastern Minnesota. *Geological Society of America Bulletin*, 94(2), 206. doi: 10.1130/0016-7606(1983)94<206:paiitk>2.0.co;2

Paces, J. B., & Miller, J., J.D. (1993). Precise U-Pb ages of Duluth Complex and related mafic intrusions, northeastern Minnesota: Geochronological insights to physical, petrogenetic, paleomagnetic, and tectonomagmatic processes associated with the 1.1 Ga Midcontinent Rift System. *Journal of Geophysical Research: Solid Earth*, 98(B8), 13997–14013. doi: 10.1029/93jb01159

Remond, G., Cesbron, F., Chapoulie, R., Ohnenstetter, D., Roques-Carmes, C., & Schvoerer, M. (1992). Cathodoluminescence applied to the microcharacterization of mineral materials: a present status in experimentation and interpretation. *Scanning microscopy*, 6(1), 2.

Rubatto, D. (2002). Zircon trace element geochemistry: partitioning with garnet and the link between U–Pb ages and metamorphism. *Chemical Geology*, 184(1-2), 123–138. doi: 10.1016/s0009-2541(01)00355-2

Schaltegger, U., Fanning, C. M., Günther, D., Maurin, J. C., Schulmann, K., & Gebauer, D. (1999). Growth, annealing and recrystallization of zircon and preservation of monazite in high-grade metamorphism: conventional and in-situ U-Pb isotope, cathodoluminescence and microchemical evidence. *Contributions to Mineralogy and Petrology*, 134(2-3), 186–201. doi: 10.1007/s004100050478

Schoene, B., Crowley, J. L., Condon, D. J., Schmitz, M. D., & Bowring, S. A. (2006). Reassessing the uranium decay constants for geochronology using

- 766 ID-TIMS U–Pb data. *Geochimica et Cosmochimica Acta*, 70(2), 426–445. doi:
767 10.1016/j.gca.2005.09.007
- 768 Schutt, D. L., Lowry, A. R., & Buehler, J. S. (2018). Moho temperature and mobil-
769 ity of lower crust in the western United States. *Geology*, 46(3), 219–222. doi:
770 10.1130/g39507.1
- 771 Self, S., Jay, A., Widdowson, M., & Keszthelyi, L. (2008). Correlation of the Deccan
772 and Rajahmundry Trap lavas: Are these the longest and largest lava flows on
773 Earth? *Journal of Volcanology and Geothermal Research*, 172(1-2), 3–19. doi:
774 10.1016/j.jvolgeores.2006.11.012
- 775 Shank, S. G. (1989). The petrology of the Beaver Bay Complex near Silver Bay,
776 northeastern Minnesota. *Minnesota, University of Minnesota*.
- 777 Sun, S.-S., & McDonough, W. F. (1989). Chemical and isotopic systematics of
778 oceanic basalts: implications for mantle composition and processes. *Geological
779 Society, London, Special Publications*, 42(1), 313–345. doi: 10.1144/gsl.sp.1989
780 .042.01.19
- 781 Swanson-Hysell, N. L., Hoaglund, S. A., Crowley, J. L., Schmitz, M. D., Zhang,
782 Y., & Miller, J. D. (2020). Rapid emplacement of massive Duluth Com-
783 plex intrusions within the North American Midcontinent Rift. *Geology*. doi:
784 10.1130/g47873.1
- 785 Swanson-Hysell, N. L., Maloof, A. C., Weiss, B. P., & Evans, D. A. D. (2009).
786 No asymmetry in geomagnetic reversals recorded by 1.1-billion-year-old Ke-
787 weenawan basalts. *Nature Geoscience*, 2(10), 713–717. doi: 10.1038/ngeo622
- 788 Swanson-Hysell, N. L., Ramezani, J., Fairchild, L. M., & Rose, I. R. (2019). Failed
789 rifting and fast drifting: Midcontinent Rift development, Laurentia’s rapid mo-
790 tion and the driver of Grenvillian orogenesis. *GSA Bulletin*, 131(5-6), 913–940.
791 doi: 10.1130/b31944.1
- 792 Tauxe, L., Shaar, R., Jonestrask, L., Swanson-Hysell, N. L., Minnett, R., Koppers,
793 A. A. P., ... Fairchild, L. (2016). PmagPy: Software package for paleomag-
794 netic data analysis and a bridge to the Magnetics Information Consortium
795 (MagIC) Database. *Geochemistry, Geophysics, Geosystems*, 17(6), 2450–2463.
796 doi: 10.1002/2016gc006307
- 797 Unsworth, J., & Duarte, F. J. (1979). Heat diffusion in a solid sphere and Fourier
798 theory: An elementary practical example. *American Journal of Physics*,

- 799 47(11), 981–983. doi: 10.1119/1.11601
- 800 van Hinsbergen, D. J. J., Steinberger, B., Doubrovine, P. V., & Gassmöller, R.
- 801 (2011). Acceleration and deceleration of India-Asia convergence since the
- 802 Cretaceous: Roles of mantle plumes and continental collision. *Journal of*
- 803 *Geophysical Research*, 116(B6). doi: 10.1029/2010jb008051
- 804 Vervoort, J. D., Wirth, K., Kennedy, B., Sandland, T., & Harpp, K. S. (2007). The
- 805 magmatic evolution of the Midcontinent rift: New geochronologic and geo-
- 806 chemical evidence from felsic magmatism. *Precambrian Research*, 157(1-4),
- 807 235–268. doi: 10.1016/j.precamres.2007.02.019
- 808 White, W. (1960). The Keweenawan lavas of Lake Superior, an example of flood
- 809 basalts. *American Journal of Science*, 258, 367–374.